International Journal of Heat and Fluid Flow 31 (2010) 141–153

Contents lists available at ScienceDirect

International Journal of Heat and Fluid Flow

journal homepage: www.elsevier.com/locate/ijhff

Wake structure for flow past and through a porous square cylinder

P. Yu *, Y. Zeng, T.S. Lee, H.X. Bai, H.T. Low

Department of Mechanical Engineering, National University of Singapore, Singapore

ARTICLE INFO

Article history:
Received 5 May 2009
Received in revised form 30 October 2009
Accepted 17 December 2009
Available online 18 January 2010

Keywords:
Fluid–porous interface
Porous square cylinder
Detached recirculating wake

ABSTRACT

Numerical simulations have been performed for the flow past and through a porous square cylinder over a wide range of Reynolds numbers ($1 \leqslant Re \leqslant 50$) and Darcy numbers ($10^{-6} \leqslant Da \leqslant 10^{-1}$). It is found that the recirculating wake existing downstream of the cylinder is completely detached from the body under a certain range of parameters. The size and the location of the wake mainly depend on Re and Da. Specially, the wake may initially increase but then decrease in size with an increase in Re, and eventually disappear when the Reynolds number is sufficiently large. The variation of the critical Reynolds number for the onset of recirculating wake as a function of Darcy number is summarized. The results also show that in the range of Da investigated, different from that of the solid cylinder, the recirculating wake is initially developed downstream of the porous cylinder, but not on the surface of it.

1. Introduction

Flow past bluff porous body occurs in many practical applications. A typical application in bioengineering is the flow system in bioreactor with porous microcarriers (Braeckmans et al., 2002) or porous scaffold (Yu et al., 2009), in which the surrounding flow should effectively transport nutrients and metabolites to and from porous structure where the cells are attached. Another application can be found in chemical process industries, which involves the settling of 'flocs' of material in liquid–solid rectors (Masliyah and Polikar, 1980; Noymer et al., 1998). Other applications include the nuclear biological chemical filters, which are widely used for chemical, pharmaceutical and medical industries (Bhattacharyya et al., 2006).

The low Reynolds number flow of viscous fluid around a porous sphere has been examined by Joseph and Tao (1964) and Neale et al. (1973). It was found that the drag on a permeable sphere is less than that for an impermeable sphere at a low Reynolds number. The steady flow around a porous cylinder at a moderate Reynolds number has been investigated by Noymer et al. (1998) and Bhattacharyya et al. (2006). Their numerical solutions implied that the wake appears and attaches to the porous cylinder under certain parameter ranges. The unsteady vortex shedding behind a porous square cylinder has also been studied by Jue (2004) and Chen et al. (2008). It was found that the onset Reynolds number for vortex shedding is delayed with an increase in Darcy number.

All the above studies suggest that the flow phenomena associated with porous cylinder are rather similar to those of solid cylinder. However, a recent work of Yu et al. (submitted for publication) revealed that the wake existing downstream of the porous circular cylinder either penetrates into or is completely detached from the cylinder, but is not attached to it. The detached wake has also been reported in other flow conditions. The first is the flow around a two-dimensional cylindrical body with "base bleed", which has been investigated by Leal and Acrivos (1969). By involving the injection of relatively low velocity fluid through the trailing edge base of the bluff body, i.e. "base bleed", the detached recirculating wake was observed at a Reynolds number of 260. The second example of a flow is the translational motion of a viscous drop (Dandy and Leal, 1989; Rivkind and Ryskin, 1976), in which the detached wake occurs in a wide range of parameters. All these evidences suggest that the appearance of recirculating wakes is not a result of separation in boundary layers in an adverse pressure gradient but may be due to vorticity accumulation as proposed by Leal (1989), and Dandy and Leal (1989).

The objective of the present study is to investigate the steady flow past and through a porous square cylinder. The main motivation is to examine whether the penetrating wake and the detached wake, which occur in the flow around the porous circular cylinder, would still appear for the square one. Also, we aim to characterize the flow behaviour, especially the wake structure, as a function of the Reynolds number and the Darcy number.

Indeed, the present simulations reveal that the wake is completely detached from the square cylinder under a certain range of parameters. Specially, the wake may initially increase but then decrease in size with an increase in the Reynolds number, and eventually disappear when the Reynolds number is sufficiently

* Corresponding author. Address: Division of Fluid Mechanics, Department of Mechanical Engineering, National University of Singapore, 9 Engineering Drive 1, 117576 Singapore. Tel.: +65 68744432; fax: +65 68742232.
E-mail address: mpeyp@nus.edu.sg (P. Yu).

0142-727X/$ - see front matter © 2009 Elsevier Inc. All rights reserved.
doi:10.1016/j.ijheatfluidflow.2009.12.009

large. Again, these features indicate that the recirculating wake at a finite Reynolds number should be viewed as 'being a consequence of vorticity accumulation rather than a finite-Reynolds-number version of the separation process that is described by boundary-layer theory for asymptotic limit $\mathrm{Re} \to \infty'$ (Leal, 1989). These new findings in turn promote us to examine, from the fundamental point of view, how vorticity is produced. The interface jump boundary condition can be regards as an intermediate condition between no-slip and zero shear stress. Thus, the mechanism of vorticity production is similar to that of a viscous drop in this sense. Moreover, as the streamline can pass through the cylinder, the normal velocity component is nonzero at the surface. This feature resembles the flow around a solid body with base bleed. The overall mechanism for the porous square cylinder is somewhat similar to that of the circular one (Yu et al., submitted for publication). However, the curvature effect of the circular cylinder is replaced by the sharp corner effect of the square one. Hence, the present study provides some insight into the competition/cooperation of the above-mentioned mechanisms.

The remainder of this paper is organized as follows: Section 2 describes the governing equations, boundary conditions, and solution techniques and presents grid-independent study and validation. Section 3 demonstrates the numerical results, which include the variations of flow pattern, especially the recirculating wake, with the Reynolds and Darcy numbers. The new findings are highlighted and their underlying mechanism is discussed in this section. And finally, in Section 4, the conclusion is drawn.

2. Computational methods

2.1. Governing equations

The computational domain is presented schematically in Fig. 1, which shows an infinite long porous square cylinder of side length D placed in a uniform flow (from left to right) with velocity U_∞. Here only the steady flow is considered and in the flow regime, the two-dimensional simulations are able to capture all flow features. To minimize the effect of the outer boundaries, the lengths of the computational domain in the streamwise and spanwise directions are defined as 60 times the side length of the cylinder. Considering two-dimensional, steady, laminar flow of an incompressible, viscous fluid, the governing equations for a homogenous fluid region, using vector form, can be written as:

$$\nabla \cdot \vec{u} = 0 \tag{1}$$

$$\rho \vec{u} \cdot \nabla \vec{u} = -\nabla p + \mu \nabla^2 \vec{u} \tag{2}$$

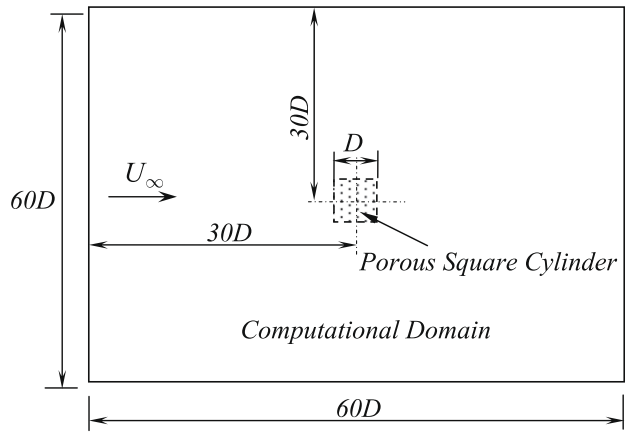

Fig. 1. Schematic of flow past a porous square cylinder.

where p is the pressure, ρ is the fluid density, and μ is the fluid dynamic viscosity.

The porous medium is considered to be rigid, homogeneous and isotropic, and saturated with the same single-phase fluid as that in the homogenous fluid region. The governing equations for porous region based on Darcy–Brinkman–Forchheimer extended model can be expressed as (Chen et al., 2008; Yu et al., 2007):

$$\nabla \cdot \vec{u} = 0 \tag{3}$$

$$\underbrace{\rho \frac{\vec{u}}{\varepsilon} \cdot \nabla \frac{\vec{u}}{\varepsilon}}_{\text{Convective Term}} = -\underbrace{\nabla p^*}_{\text{Pressure Term}} + \underbrace{\frac{\mu}{\varepsilon} \nabla^2 \vec{u}}_{\text{Brinkman Term}} - \underbrace{\frac{\mu}{K} \vec{u}}_{\text{Darcy Term}} - \underbrace{\frac{\rho C_F |\vec{u}|}{\sqrt{K}} \vec{u}}_{\text{Forchheimer Term}} \tag{4}$$

where $\vec{u}$ is the local average velocity vector (Darcy velocity), p^* is the intrinsic average pressure, μ is the fluid dynamic viscosity, ε is the porosity, K is the permeability, and $C_F \left(= 1.75/\sqrt{150\varepsilon^3}\right)$ is Forchheimer coefficient. Note that throughout the paper, viscosity means dynamic viscosity of the fluid but not the effective (Brinkman) viscosity. The "*" denotes the intrinsic average, which is an average over the volume occupied by the fluid phase. The local average and intrinsic average can be linked by the Dupuit–Forchheimer relationship, for example, $p = \varepsilon p^*$.

The stress jump condition (Ochoa-Tapia and Whitaker, 1995a,b, 1998) is applied at the porous–fluid interface:

$$\frac{\mu}{\varepsilon} \frac{\partial u_t}{\partial n}\bigg|_{\text{porous}} - \mu \frac{\partial u_t}{\partial n}\bigg|_{\text{fluid}} = \beta_1 \frac{\mu}{\sqrt{K}} u_t \bigg|_{\text{interface}} + \beta_2 \rho u_t^2 \tag{5}$$

where in the porous medium region, u_t is the Darcy velocity component parallel to the interface aligned with the direction t and normal to the direction n while in the homogenous fluid region u_t is the fluid velocity component parallel to the interface; β_1 and β_2 are adjustable parameters which account for the stress jump at the interface.

The stress jump condition is based on a generalized nonlocal form of the volume average Navier–Stokes equations, which accounts for the excess surface stress encountered at the interface. β_1 is a coefficient associated with an excess viscous stress while β_2 is a coefficient related to an excess inertial stress. Ochoa-Tapia & Whitaker's experiment (1995b) and analysis (1998) indicated that both β_1 and β_2 are of order 1.

In addition to Eq. (5), the continuity of velocity and normal stress prevailing at the interface is given by:

$$\vec{u}|_{\text{fluid}} = \vec{u}|_{\text{porous}} \tag{6}$$

$$\frac{\mu}{\varepsilon} \frac{\partial u_n}{\partial n}\bigg|_{\text{porous}} - \mu \frac{\partial u_n}{\partial n}\bigg|_{\text{fluid}} = 0 \tag{7}$$

where in the porous medium region, u_n is the Darcy velocity component normal to the interface; and in the homogenous fluid region, u_n is the fluid velocity component normal to the interface.

For the present type of flow problems, the physical domain is infinite while the simulation must be performed on a confined computational domain. Thus the computational domain should be truncated from the real domain by using artificial open boundary conditions (Sohankar et al., 1998). In the present study, the free-stream condition on the velocity is imposed on the upstream boundary, a Neumann condition for the velocity is specified at the downstream boundary that corresponds to the stress-free condition, and the slip boundary condition is applied on the lateral boundaries.

The present study considers two-dimensional steady flow past and through a porous square cylinder with zero angle of incidence placed in a uniform free stream. The flow behaviour is determined by many factors including the Reynolds number, the Darcy

number, the porosity, jump parameters etc. The Reynolds number is based on the free-stream velocity U_∞ and the side length D:

$$\mathrm{Re} = \rho U_\infty D/\mu \tag{8}$$

The Darcy number is defined as:

$$\mathrm{Da} = K/D^2 \tag{9}$$

One of practical applications related to the present flow configuration is the cell culture in a bioreactor with porous scaffold. In this condition, the flow is usually kept laminar and steady to maintain a suitable environment for cell growth. Thus, the range of Re investigated is within 50. The flow behaviour can be fully captured by 2D simulations as the 3D transition occurs at a higher $\mathrm{Re} \sim \mathrm{O}(100)$.

The Darcy number is varied in a wide range from 10^{-6} to 10^{-1} in the present study. For the scaffold for cell culture, the permeability is in the range of 10^{-12}–10^{-9} m^2 (Yu et al., 2009), which corresponds to Da ranged from 10^{-10} to 10^{-4}, depending on the reference length used. Generally, Da may not go up to 10^{-2} in practical applications (Large, 1992). However, the upper limit of Da herein is extended to 10^{-1} from an academic point of view. For a very low Da, the porous cylinder approaches to a solid one. Thus, the lower limit of Da is set to 10^{-6}, and below this value, the effect of Da on the external flow around the porous cylinder can be negligible.

For flow past a porous cylinder, the overall flow behaviour is determined by the interaction between the external flow around and the internal flow through it. Generally, the flow around a bluff body is mainly affected by Re. The ability of a porous medium to conduct fluid flow can be quantitatively represented by the permeability, or the dimensionless Darcy number. Thus, the present flow is chiefly determined by Re and Da while other parameters have relatively small influences. The previous studies (Bhattacharyya et al., 2006; Chen et al., 2008; Yu et al., submitted for publication) have also shown that the Reynolds number and the Darcy number have dominate effects on these types of flows. Thus, the present study will focus on evaluating the effect of Re and Da. The porosity is fixed at 0.7 and the jump parameters β_1 and β_2 were both set to zero unless specified otherwise, within the range of porosity from 0.6 to 0.95 (Yu et al., 2009) and the range of jump parameters of order 1.

It is well known that for a laminar, steady flow past a bluff body, a recirculating wake consisting of a counter-rotating vortex pair may be observed behind the body for a certain range of Re. usually, the recirculating wake is fully attached to the body. For the case of a solid square cylinder, the flow separates at the trailing edges and reattaches at the centre of the leeward surface. However, in the present study, it is found that a recirculating wake behind a porous cylinder is not attached to the rear of it. The recirculating wake is either detached from or penetrates into the cylinder. This means that there is no reattachment of the recirculating wake on the surface of porous body. As illustrated in Fig. 2, the geometrical parameters considered here are the downstream distances to the leading and trailing edges of the recirculating wake (L_L and L_R), and the position of the wake centre (C_x and C_y). The length of the recirculating wake is then calculated as $L_w = L_R - L_L$. The negative value of L_L means that the recirculating wake penetrated into the cylinder.

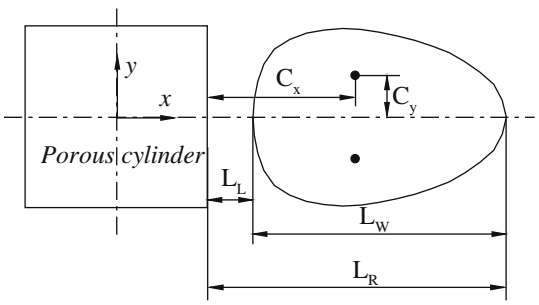

Fig. 2. Geometrical parameters of the recirculating wake behind a porous square cylinder.

The occurrence of recirculating wake is a continuous process with an increase in Re, which is determined by monitoring the stagnation points around the wake region. Recirculating wake is deemed to form when two stagnation points are observed with Re gradually increasing in steps of 1 for a fixed Da.

2.2. B. Grids-Independent study and validation

The present numerical method is based on finite volume method with a collocated variable arrangement (Ferziger and Perić, 1999). The body-fitted and multi-block grids method proposed by Lilek et al. (1997) was applied. The detailed numerical treatment can be found in Yu et al. (2007). The present numerical method has been successfully applied for flows past and around porous bluff bodies (Chen et al., 2008; Yu et al., 2007, submitted for publication). Here only a simple study is provided for validation.

A typical example of mesh within and around the porous–fluid interface is shown in Fig. 3. The whole computational domain was divided into two sub-domains, with domain 1 for the porous cylinder and domain 2 for the outer flow region. Domain 2 was meshed using O-type grid, with the grids in the radial direction stretched through an exponential progression to ensure a fine grid near the porous–fluid interface. Note that only a small part of domain 2 is shown in Fig. 3 in order to clearly illustrate the grid topology.

The present method was first applied to simulate the flow around solid square cylinder. The variation of the overall wake length L_R (distance from the rear of cylinder to the trailing edge of the recirculating wake) with Re is presented in Fig. 4, which shows good agreement with previously published results (Sharma and Eswaran, 2004). To further validate the present method, a study was performed to investigate the relationship between the overall wake length L_R and Da for a porous square cylinder at fixed Re = 20 and $\varepsilon = 0.7$. Fig. 5 shows that the overall wake length L_R becomes longer with a decrease in Da. However the overall wake length L_R approaches a constant value at a low Da as the porous cylinder tends to a solid one. The overall wake length L_R at $\mathrm{Da} = 1 \times 10^{-6}$ is about 1.297 (Fig. 5), which is rather close to the value of 1.310 for the solid one.

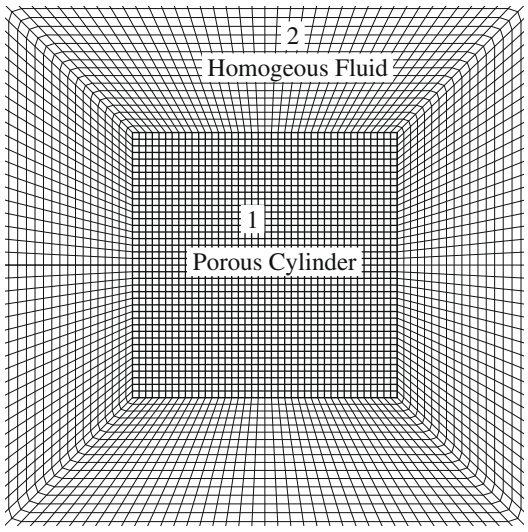

Fig. 3. A typical example of grid near the interface.

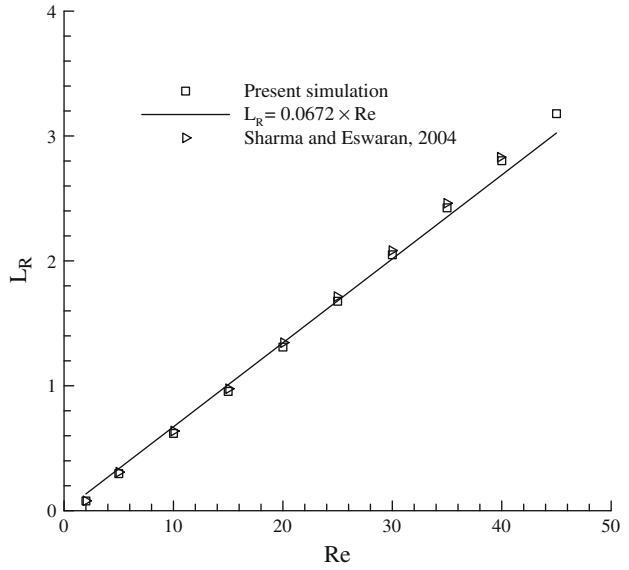

Fig. 4. Variation of wake length with Reynolds number, solid square cylinder.

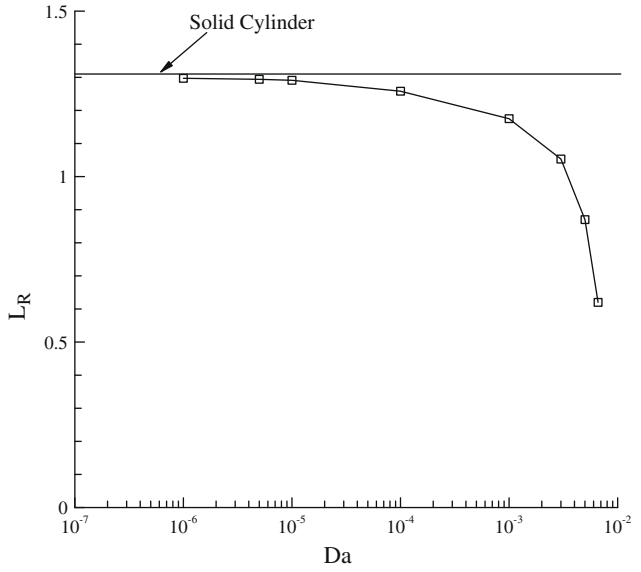

Fig. 5. Variation of overall wake length with Darcy number at Re = 20.

To ensure a grid-independent solution and accurate resolution in space, a study has been performed with three sets of mesh for both solid and porous cylinders. The tested Reynolds numbers were 20 and 45 while the Darcy number for the porous cylinder is fixed at 5×10^{-6}. Table 1 shows the comparison of L_R at various grid sizes. For the solid cylinder, the difference in L_R between the two sets of grids 320×240 and 240×200 is less than 1.5%. The results indicate that the 240×200 grid is fine enough to mesh the region outside the cylinder. For the porous cylinder, the difference in L_R between the two sets of grids (cases 5 and 6) is less than 1.5%. To ensure grid-independent solution, the grid used in case 6 was chosen for the final simulations.

3. Results and discussion

3.1. Flow pattern

The effects of Re and Da on the flow pattern are illustrated by presenting a series of streamline plots at various values of Re for four different Da. The four Darcy numbers are 10^{-2}, 7×10^{-3}, 3×10^{-3}, and 10^{-5}, with the first one for high Da value, the last one for low Da value and the rest two for intermediate Da values. As illustrated below, for different Da, the interactions between the external flow around and the internal flow within the porous cylinder are different, resulting in different flow behaviours.

Fig. 6 shows the flow field at $Da = 10^{-2}$ for several values of Re. At this high Darcy number value, the flow experiences little resistance when it passes through the porous cylinder. As a significant portion of fluid penetrates through the porous cylinder, the streamlines around it exhibits a smaller deviation compared with that around the solid cylinder. Figs. 6a to d show that the streamlines become flatter with an increase in Re. This is expected when we examine the resistance force that the internal porous flow experiences. The Darcy drag force $\mu\varepsilon\vec{u}/K$ is the main source of the resistance force, which decreases with an increase in Da or Re. As a result, the streamlines are less deviated with an increase in Da or Re.

There is no recirculating wake behind the square cylinder in the range of Re investigated for a high Darcy number. For a high Da, the shape of the object has a small effect on streamline contours. The present flow behaviour is rather similar to that of a porous circular cylinder at the same Re and Da (Yu et al., submitted for publication). In this sense, the overall flow behaviour for a high Da is mainly determined by the internal porous flow.

Now we consider the flow field at a low Darcy number. The Darcy number of 10^{-5} was chosen to show the flow behaviour at this low extreme. As shown in Fig. 7, the streamline contours at different Re indicate that the flow field resembles that around a solid cylinder. For the purpose of comparison, the streamline contours for the flow around a solid square cylinder are shown in Fig. 8. Fig. 7 shows that the recirculating wake exists at Re = 5 and increases in size with an increase in Re. At higher Re, the wake is fixed by two of the sharp edges. The lengths of the wake are 1.291 for Re = 20 and 2.772 for Re = 40, which are pretty close to those of a solid square cylinder (1.310 for Re = 20 and 2.802 for Re = 40). It is worth noting that the wake is detached from the porous square cylinder for the Reynolds number just above that for the onset of the wake. However, at high Re, the wake appears to

Table 1
Effect of grid size on the overall wake length.

	Cases	Grid size		L_R	
		Domain 1	Domain 2	Re = 20	Re = 45
Solid cylinder	1		160×160	1.285	3.023
	2		240×200	1.303	3.135
	3		320×240	1.310	3.179
Porous cylinder	4	40×40	160×160	1.262	2.982
	5	60×60	240×200	1.285	3.105
	6	80×80	320×240	1.294	3.152

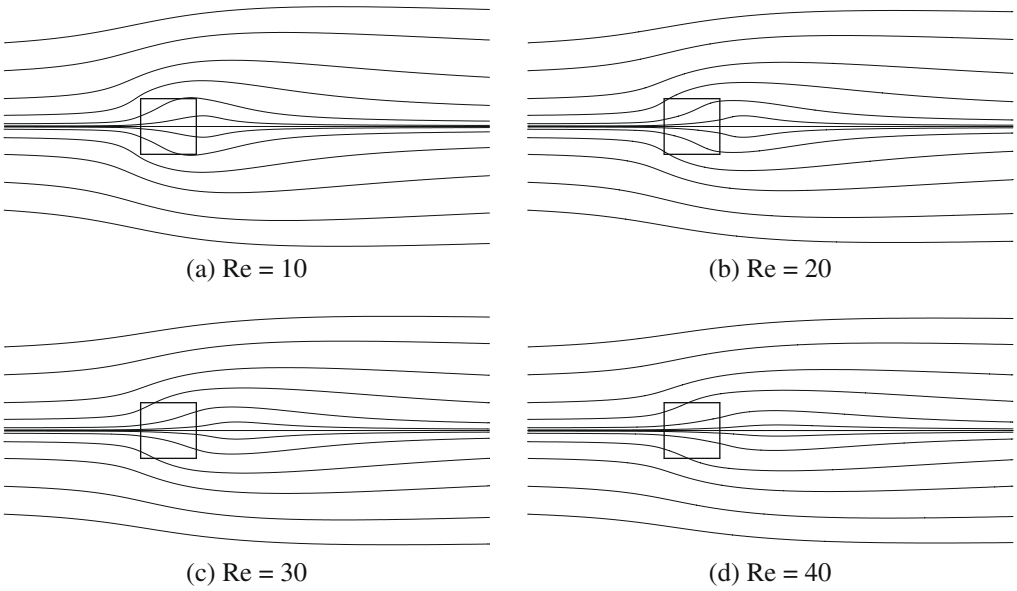

Fig. 6. Contours of streamline at a fixed Darcy number of Da = 1×10^{-2} for different Reynolds numbers as indicated.

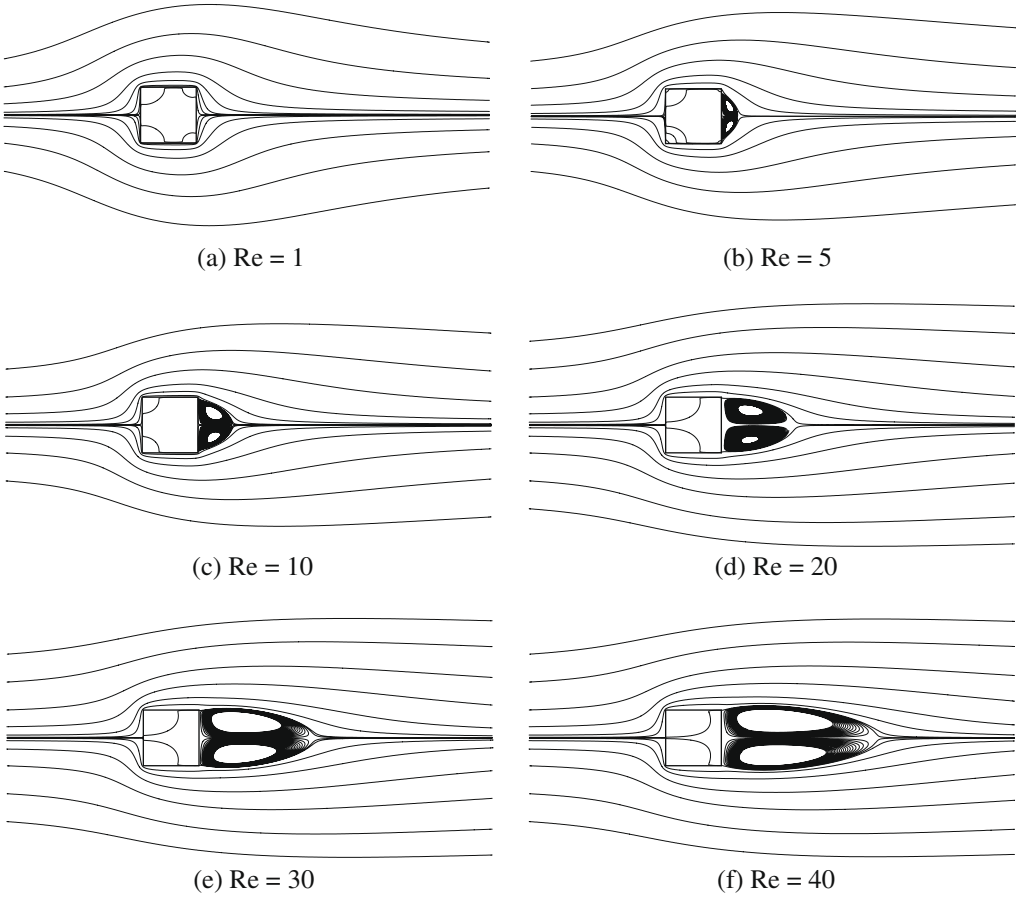

Fig. 7. Contours of streamline at a fixed Darcy number of Da = 1×10^{-5} for different Reynolds numbers as indicated.

be attached to the leeward surface so that no fluid passes through the leeward surface. In summary, the porous cylinder approaches a solid one for a low Da. The flow resistance is very large and little fluid can pass through the cylinder. Thus, the overall flow behaviour for a low Da is chiefly determined by the Reynolds number.

For an intermediate Da, the flow patterns are more complicated. At Da = 7×10^{-3}, a considerable portion of fluid penetrates through the porous square cylinder. The most striking flow feature at this Darcy number is the detached recirculating wake as shown in Figs. 9d–g. The wake first appears at a Reynolds number of

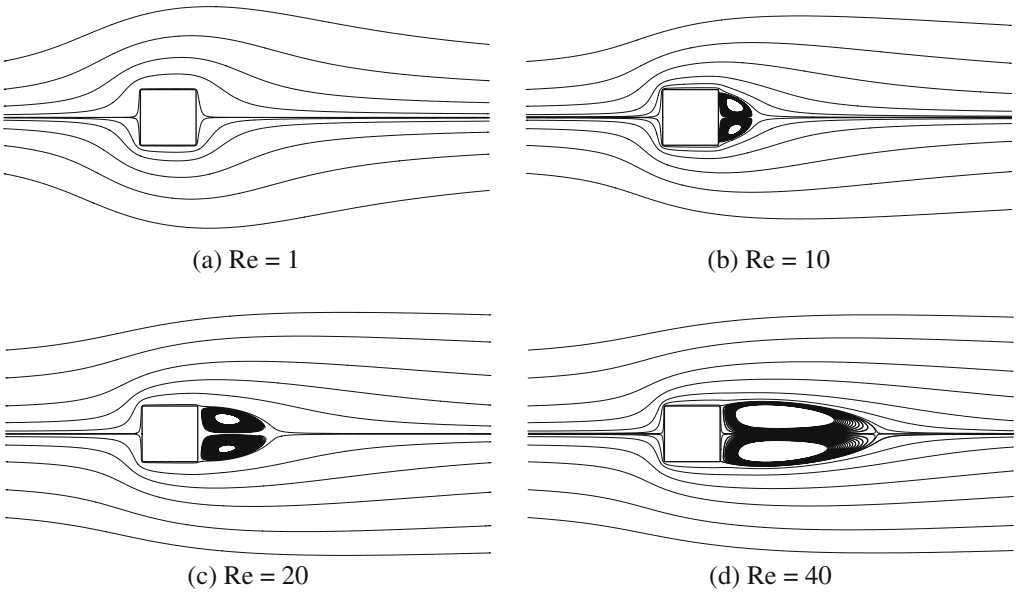

Fig. 8. Contours of streamline around a solid cylinder for different Reynolds numbers as indicated.

approximately 21, then grows to a maximum length at roughly Re = 30, decreases in size with a further increase in Re, and eventually completely disappears when the Reynolds number reaches 42. This flow behaviour on the disappearance of the detached wake is fairly similar to that of a viscous drop (Dandy and Leal, 1989). However, it occurs at $Re \sim O(100)$ for a viscous drop while at $Re \sim O(10)$ for the present porous square cylinder.

When the Darcy number goes to a relatively low value, i.e. $Da = 3 \times 10^{-3}$, the wake first appears at a Reynolds number of approximately 10. It is found that the wake grows in size but does not disappear with a continuous increase in Re as demonstrated in Fig. 10. This observation confirmed that the wake will not disappear with an increase in Re if the Darcy number is lower than a certain threshold, which is consistent with the previous studies showing that vortex shedding does occur for $Da = 1 \times 10^{-4}$ when the Reynolds number is beyond a certain critical value (Jue, 2004; Chen et al., 2008).

The detached wake has also been reported in other flow conditions. The similar case is that the flow past and through a porous circular cylinder. In the study of Yu et al. (submitted for publication), the wake existing downstream of the porous circular cylinder is found to be completely detached from the cylinder in a certain range of parameters. Another example is the translational motion of a viscous drop (Dandy and Leal, 1989; Rivkind and Ryskin, 1976), in which the detached wake may even disappear with an increasing Re. Additionally, the detached wake has also been found in the flow around a bluff body with "base bleed" studied by Leal and Acirvos (1969).

Although the detached recirculating wake structure has been observed in other fluid conditions, it is nevertheless rather remarkable comparing with the conventional attached wakes existing on solid bodies, and both bubbles and voids. When the detached wake occurs, there is not even a separation or a detachment point on the bodies, but only one "separation" point along the horizontal axis. It is also observed that the magnitude of the surface vorticity must exceed a minimum threshold level (dependent on Re) before a recirculating wake appears, which is approximately independent of the boundary condition at the surface (Leal, 1989). Based on the numerical and experimental observations of the detached recirculating wake (Leal and Acrivos, 1969; Dandy and Leal, 1989; Rivkind and Ryskin, 1976), Leal (1989) concluded in his pioneer work that 'Recirculating wakes form at finite Reynolds number due to vorticity accumulation, and this has nothing to do with the mechanics of boundary layer separation in the limit $Re \to \infty$'.

For flow past a smooth bluff body, vorticity is generated by two mechanisms, i.e. the no-slip boundary condition and the surface curvature. It is shown that the dimensionless vorticities generated by surface curvature and by the no-slip condition are O(1) and $O(Re^{1/2})$ for large Re, respectively (Leal, 1989). For the porous circular cylinder, the rate of vorticity production results from the corporation/competition of the two mechanisms (Yu et al., submitted for publication). For the porous square cylinder, there is no smooth surface curvature but sharp edge. The recirculating wake first occurs around Re = 1 for a solid square cylinder (Sharma and Eswaran, 2004; Zaki, 1994) whilst it first occurs around Re = 6 for a solid circular one (Yu et al., submitted for publication; Underwood, 1969), which suggest that the sharp edge is a more effective source of vorticity generation compared with the no-slip condition. Note that the flow passes through the porous square cylinder and the exiting flow at the leeward surface resembles 'base bleed'. This 'base bleed' also has a significant effect on the flow behaviour. We shall give more discussion on this aspect later.

To provide a quantitative analysis, we present a series of vorticity plots at various values of Re for different Da. Fig. 11 shows the vorticity contours at Re = 1 and 5 for $Da = 1 \times 10^{-5}$, which demonstrates that the vorticity is accumulated around the leading edges of the cylinder. For Re = 5, the magnitude of vorticity significantly increases comparing with that of Re = 1 (7.9 for Re = 5 while 3.8 for Re = 1). This means that with Re increasing, the generation rate of vorticity is faster than the convection rate. When the magnitude of vorticity exceeds a certain threshold, the recirculating wake is induced. However, when Da is increased, more fluid may penetrate the porous cylinder, resulting in an increase in the convection rate of vorticity. Fig. 12 shows the vorticity contours at Re = 35 and 45 for $Da = 7 \times 10^{-3}$. Now the magnitude of vorticity decreases with increasing Re as shown in Figs. 12a and b, implying that the convection rate of vorticity is fast than the generation rate. Thus, the recirculating wake disappears at Re = 45 because vorticity is not sufficiently strong.

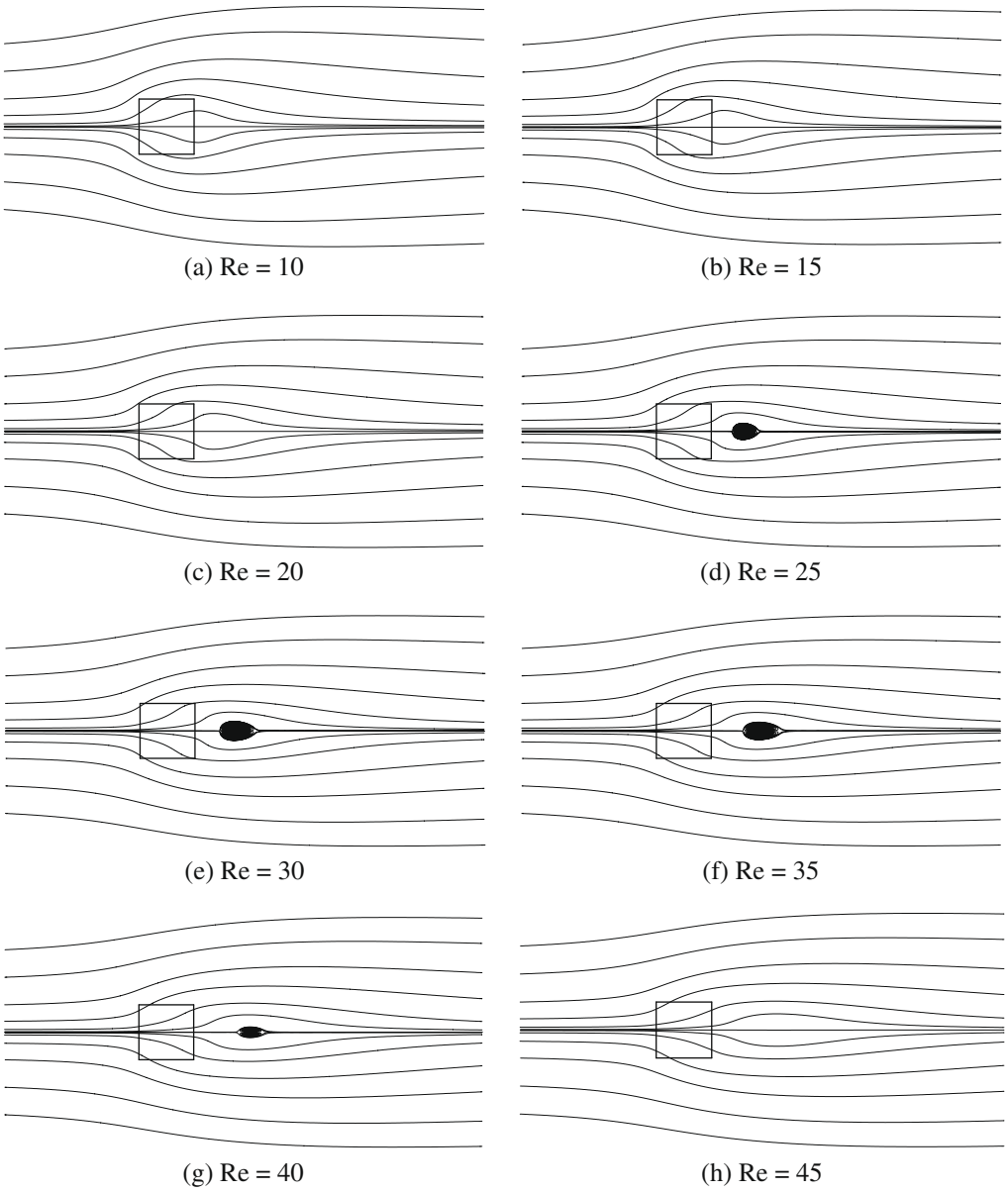

Fig. 9. Contours of streamline at a fixed Darcy number of $Da = 7 \times 10^{-3}$ for different Reynolds numbers as indicated.

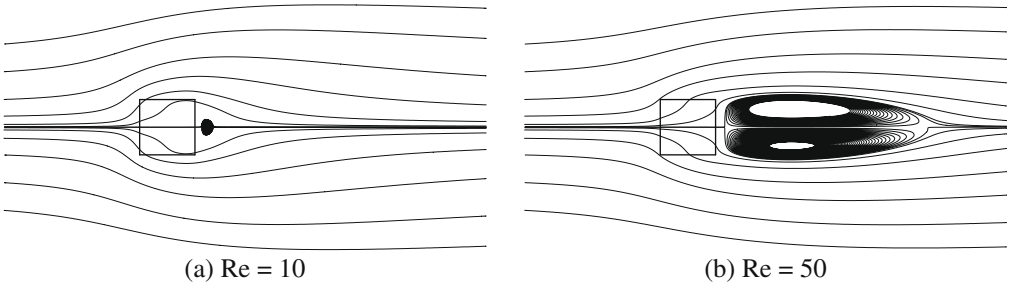

Fig. 10. Contours of streamline at a fixed Darcy number of $Da = 3 \times 10^{-3}$ for different Reynolds numbers as indicated.

3.2. Occurrence of recirculating wake

Now the attention focuses on the effect of Da on the critical Reynolds number for the occurrence of a recirculating wake. As shown in Fig. 13, the critical Reynolds number decreases with decreasing Da. There is no recirculating wake in the range of Re investigated when $Da > 7.5 \times 10^{-3}$. The recirculating wake first appears around $Re_{cr} = 24.5$ for $Da = 7.4 \times 10^{-3}$. The critical Reynolds number rapidly decreases to 5.5 for $Da = 10^{-3}$ and slowly drops to 1.5 for $Da = 10^{-6}$. Fig. 13 suggests that when Da goes to an infinitely small value, the critical Reynolds number approaches an asymptote which equals to that of a solid cylinder.

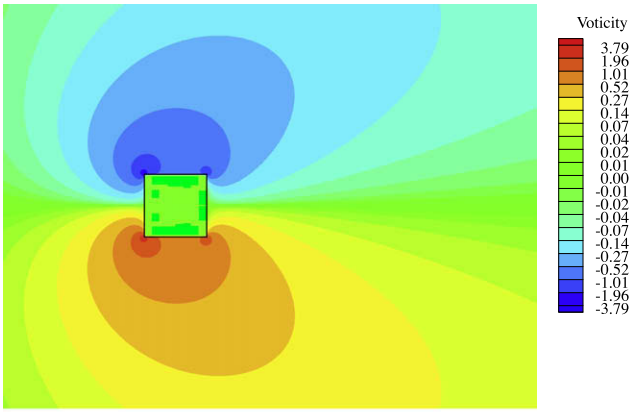

(a) Re = 1

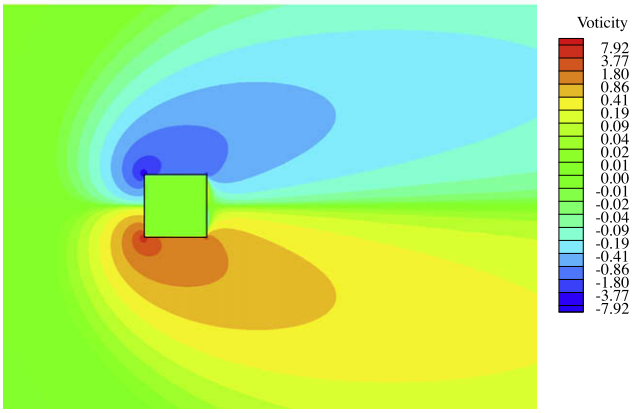

(b) Re = 5

Fig. 11. Contours of vorticity at a fixed Darcy number of Da = 1 for different Reynolds number as indicated.

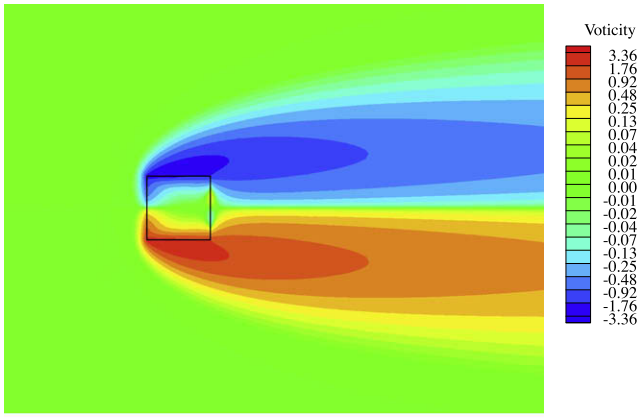

(a) Re = 35

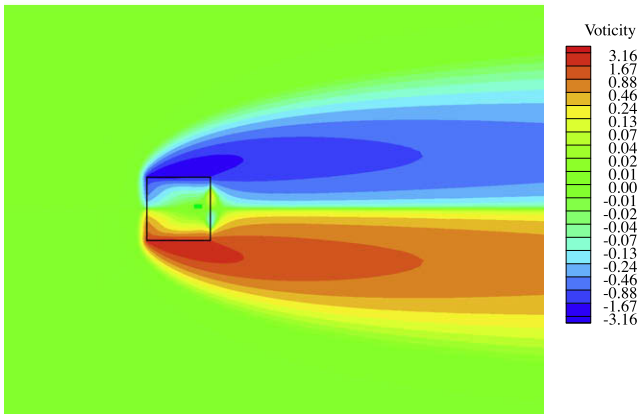

(b) Re = 45

Fig. 12. Contours of vorticity at a fixed Darcy number of Da = 7 for different Reynolds number as indicated.

The present simulation indicates that the critical Reynolds number for a solid cylinder is around 1.5, which is consistent with the results of Zaki et al. (1994) and of Sharma and Eswaran (2004).

Fig. 13 also presents the variations of the critical Reynolds number for the disappearance of a recirculating wake. For $Da = 7.4 \times 10^{-3}$, the recirculating wake disappears at $Re_{dis} \approx 33.5$. With decreasing Da, the recirculating wake disappears at a higher Re, for example at $Re_{dis} \approx 48.5$ for $Da = 6.6 \times 10^{-3}$. The disappearance phenomenon of a recirculating wake only occurs at a narrow range of Da. For an even lower $Da = 10^{-4}$, the recirculating wake does not disappear.

Fig. 14 presents the streamlines for the flow around and through the porous square cylinder at the Reynolds number slightly larger than the critical Re for the onset of the recirculating wake. The streamline contours clearly show that, for all the three Darcy numbers $Da = 7 \times 10^{-3}$, 1×10^{-3} and 1×10^{-5}, the recirculating wake is not separated from the surface of it. Fig. 14a shows that the wake initially occurs around 0.4D downstream of the cylinder at $Da = 7 \times 10^{-3}$. For a lower Da of 1×10^{-3}, the wake moves towards the rear of square cylinder as shown in Fig. 14b. For an even lower Da of 1×10^{-5}, the recirculating wake almost attaches to the rear of the cylinder (Fig. 14c). This trend indicates that when the Darcy number tends to an infinitely small value, that is the porous cylinder approaches a solid one, the recirculating wake eventually attaches to the rear of square cylinder. Clearly, when the wake initially occurs, there is only one "separation" point along the horizontal axis outside the porous square cylinder, but not a pair of separation points as what exit on the surface of the solid cylinder or bubble/void (Dandy and Leal, 1986).

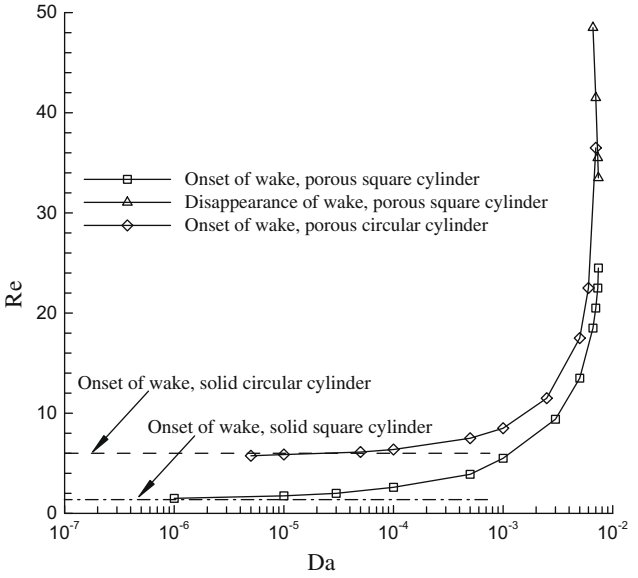

Fig. 13. Variation of critical Reynolds numbers for onset and disappearance of recirculating wake with Darcy number.

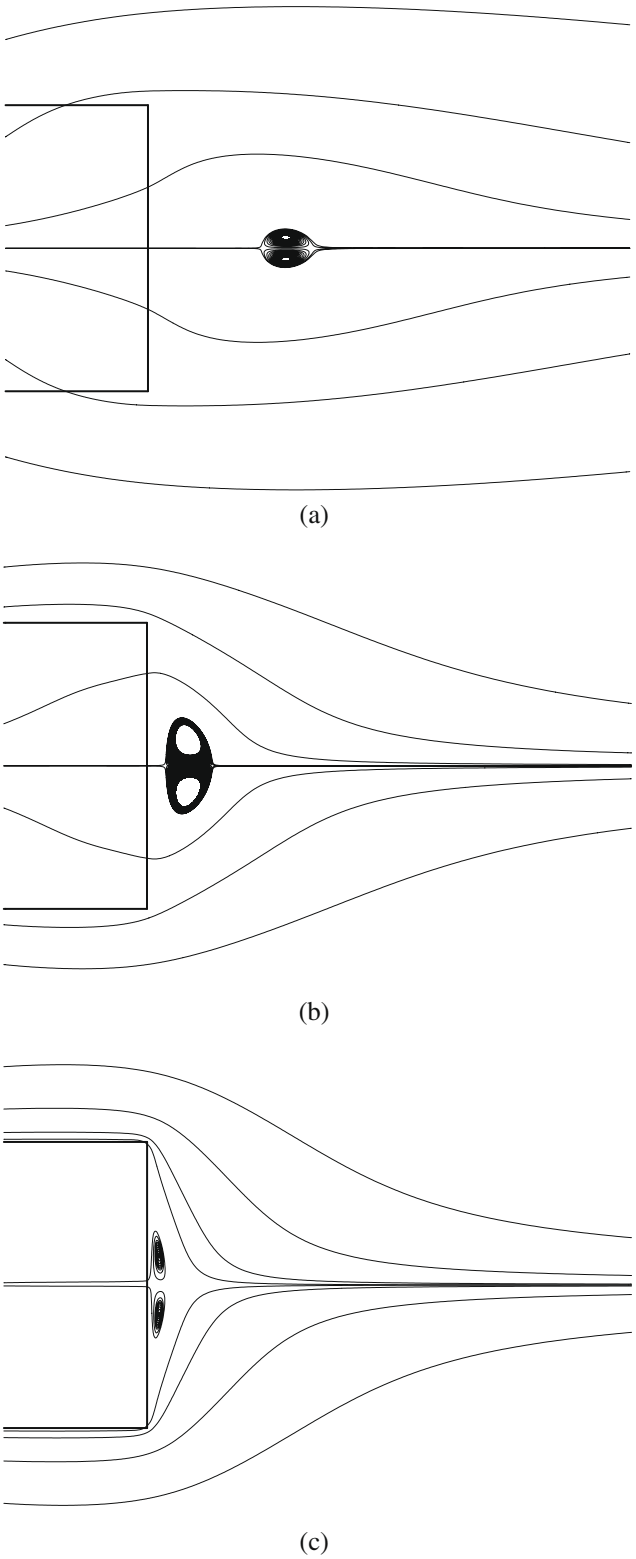

Fig. 14. Streamlines for the flow around and through the porous square cylinder just after the formation of recirculating wake; (a) Re = 21, Da = 7×10^{-3}; (b) Re = 6, Da = 10^{-3}; and (c) Re = 2, Da = 10^{-5}.

It has been found that the detached wake may also appear behind a porous circular cylinder (Yu et al., submitted for publication). The flow behaviours behind the two different shapes of cylinders share some common characteristics. For example, a recirculating wake never occurs if the Darcy number is beyond a certain value (around 7×10^{-3}). The critical Reynolds number for the onset of a recirculating wake tends to that of a solid cylinder with the same shape when the Darcy number approaches an infinitely small value.

For the flow past a porous body, the fluid velocity along the surface, which is mainly determined by the Darcy number and Reynolds number, and secondly affected by the jump parameters, is nonzero. Compared with that of the solid cylinder, this velocity changes the rate of vorticity production on the surface. Also, it influences the transport of vorticity along the shear layer that exists behind the body. Thus, different from the attached wake existing on solid bodies, and both bubbles and voids, the recirculating wake is now detached from the porous surface.

Specially, the normal velocity component along the leeward surface of porous square cylinder resembles 'base bleed'. Fig. 15 shows the normal velocity component along the leeward surface at different Da for Re = 20. The velocity reaches the maximum value at the two sides and the minimum value at the centre. Near the centre of the surface, the velocity profile is rather flat, especially when the Darcy number is small. The velocity is larger when the Darcy number is bigger, and so does the difference between the velocities at the side and the centre.

According to the entrainment–detrainment mechanism (Leal and Acrivos, 1969), the recirculating wake behind bluff body is primarily due to the flow field that results from fluid being entrained into the inner side of this shear layer. The entrained fluid detrains and reverses itself in the direction to supply the entrainment needs of the shear layer. This description has been used to discuss the effects of base bleed on the wake structure by Leal and Acrivos (1969). It is also suitable to explain the effect of the normal velocity component along the leeward surface ('base bleed' velocity) in the present study. As shown in Fig. 15, the 'base bleed' velocity is small if the Darcy number is relatively small. Thus, the amount of fluid being supplied into the near-wake is not sufficient to satisfy the entrainment needs of the shear layer along the detached streamline, and the recirculating wake should form downstream. However, if the 'base bleed' velocity is large due to a relatively large Da and the sufficient amount of fluid is supplied into the near-wake, the recirculating wake should disappear.

The above explanation is consistent with the tendency of the Re_{cr}–Da Curve as shown in Fig. 13. At an extremely high Da, the

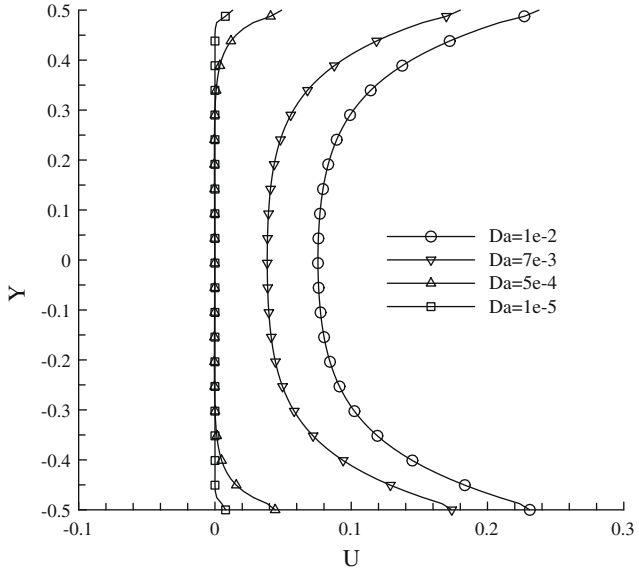

Fig. 15. Normal velocity component along the leeward surface at different Da for Re = 20.

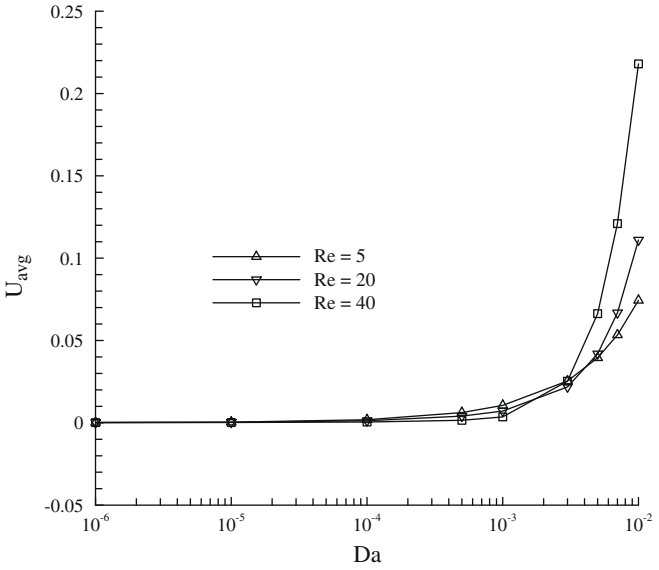

Fig. 16. Average normal velocity U_{avg} along the leeward surface of the porous square cylinder for different Re and Da.

recirculating wake may not appear in the range of Re investigated due to a high 'base bleed' velocity. At an extremely low Da, the critical Reynolds number approaches that of the solid cylinder due to a zero 'base bleed' velocity. At an intermediate Da, the critical Reynolds number is larger than that of the solid cylinder due to a moderate 'base bleed' velocity.

To provide a somewhat quantitative analysis, we summarize the average normal velocity U_{avg} along the leeward surface of the porous square cylinder for different Re and Da. This average velocity can be also regarded as the 'base bleed' rate. As seen in the plot in Fig. 16, for fixed Re, U_{avg} increases with an increase in Da, which means more fluid being supplied into the near-wake. Thus a high Reynolds number is needed to cause a recirculating wake at a high Da. If the amount of the fluid is sufficient to satisfy the entrainment needs of the shear layer at an even higher Da, a recirculating wake should be absent. The present simulation indicates that for a high $Da > 7.5 \times 10^{-3}$, the 'base bleed' rate is larger than around 0.05, at which condition the recirculating wake does not appear. Similarly, the early experiments conducted by Bearman (1967) and Leal and Acrivos (1969) have indicated that the recirculating wake behind a two-dimensional bluff body has effectively disappeared if the 'base bleed' rate is beyond a certain threshold of ~0.15. It is also similar to the numerical simulations of Arcas and Redekopp (2004), which showed that the vortex shedding behind the blunt body is suppressed when the critical bleed coefficient is beyond a certain critical value.

However, the Darcy number is not the sole factor that determines the 'base bleed' rate. Fig. 16 shows that the Reynolds number also has noticeable effect on the 'base bleed' rate. At a fixed value of Da, with an increase in Re, the 'base bleed' rate increases when $Da > 5 \times 10^{-3}$ while decreases when $Da < 1 \times 10^{-3}$. Thus, the detached wake can only be understood from the interaction between the external flow, which is mainly determined by the Reynolds number and the body shape, and the internal porous flow, which is mainly determined by the Reynolds number and Darcy number.

At a high Da, the 'base bleed' rate increases with an increase in Re, which would in turn affect the onset of recirculating wake. If a significant portion of flow, characterized by a dimensionless value of q, passes through the cylinder, the effective Reynolds number for flow around the cylinder is decreased to $Re_{eff} = (1 - q)Re$. In this sense, a relatively larger Reynolds number is needed to induce the recirculating wake. Thus, at a high Da, both Da and Re themselves primarily determine the critical Reynolds number for onset of a recirculating wake. However, at a very low Da, the 'base bleed' rate is negligible and the detached wake is mainly influenced by the external flow. The limit $Da \to 0$ can be regarded as a solid cylinder and the critical Reynolds number for onset of a recirculating wake is equal to that of the solid cylinder.

Now it is not surprising to observe the disappearance of recirculating wake with a further increase in Re when $6.6 \times 10^{-3} < Da < 7.4 \times 10^{-3}$ (see Fig. 13). In this range of Da, the 'base bleed' rate increases with Re (see Fig. 16). If the 'base bleed' rate exceeds a certain threshold, the amount of bleeding fluid is sufficient to satisfy the entrainment needs and the recirculating wake disappears. Hence, in this range of Da, the recirculating wake decreases in size and eventually disappears with a continuous increase in Re.

It is worth noting that the noticeable differences exist between the flow behaviours behind the porous square and circular cylinders, due to the shape effect. Clearly, at the same Darcy number, the critical Reynolds number for onset of a recirculating wake of the porous square cylinder is smaller than that of the porous circular cylinder as shown in Fig. 13. As explained above, this is because the sharp edge of the square cylinder is more effective on vorticity generation compared with the smooth curvature of the circular one.

Nevertheless, Yu et al. (submitted for publication) did not observe the disappearance of the recirculating wake behind the porous circular cylinder with an increase in Re. One possible reason is that for the porous circular cylinder the effect of Re on the 'base bleed' rate is smaller than that of the porous square cylinder. Also, the range of Re in the work of Yu et al. (submitted for publication) is limited to be within 40. The disappearance of the recirculating wake might be observed if they continuously increased the Reynolds number to a relatively high value.

Another interesting difference is the asymptotic behaviour of the critical Reynolds number with a continuous decrease in Da. For the porous square cylinder, the critical Reynolds number monotonically decreases to the asymptotic value of the solid square cylinder with a decrease in Da. However, for the porous circular cylinder, with decreasing Da, the critical Reynolds number may initially decrease to a value lower than, and then asymptotically increase to, that of a solid circular cylinder (Yu et al., submitted for publication). Yu et al. (submitted for publication) explained that the unexpected trend of the Re_{cr}–Da curve for the porous circular cylinder might be caused by the negative exit velocity at the rear of the cylinder, that is the 'base suction' effect. However, in the present study, Fig. 16 shows that the 'base bleed' rate from leeward surface of the porous square cylinder is always large than zero and monotonically approaches zero with a continuous decrease in Da.

Furthermore, the recirculating wake always initially develops outside of the porous square cylinder while may initially occur inside of the porous circular cylinder for a certain range of Da. Other minor difference includes that the largest Darcy number of the onset of a recirculating wake for a porous square cylinder is slightly larger than that for a porous circular cylinder. As explained above, the sharp edge of the porous square cylinder might cause these differences.

The detached wake has also been observed behind a viscous drop (Dandy and Leal, 1989). This detached wake may also disappear with a continuous increase in Re. Based on the detailed numerical simulations, Dandy and Leal (1989) concluded that these flow behaviours are controlled by the weak motion of the fluid inside the viscous drop. Similarly, in the present study, a small mount of fluid passes through the porous cylinder, which causes the same behaviour of the recirculating wake. Both of the studies indicates that the necessary condition of the occurrence of

detached wake is the weak motion of the fluid existing inside the bluff body, which appears to control the behaviour of the external flow near the body. The difference of the two flows is that the fluid only recirculates inside the viscous drop while it penetrates through the porous cylinder. In this sense, this penetrating flow is more similar to the base bleed effect (Leal and Acrivos, 1969).

The critical Reynolds number for onset of the detached wake behind the viscous drop occurs at Re $\sim$ O(10), which is the same order as that of the solid sphere. The critical Reynolds number for the onset of a recirculating wake behind a porous cylinder occurs at Re $\sim$ O(1), which is the same order as that of its solid pair. Specially, when Da $\to$ 0, this critical Reynolds number approaches exactly that of the solid pair. This suggests that, although the exact value of the critical Reynolds number for a porous cylinder is different from that of the solid one, the underlying physics of the detached or penetrating wake behind the porous cylinder should be the same as that of the solid one. The observations that the recirculating wake develops downstream of the porous square cylinder and there is only one "separation" point along the horizontal axis outside the porous cylinder as shown in Fig. 14 further support the conclusion on vorticity accumulation as suggested by Leal (1989), and Dandy and Leal (1989).

3.3. Geometrical parameters of recirculating wake

The downstream distances to the leading and trailing edges of the recirculating wake (L_L and L_R) are plotted against Re with Da as a parameter in Fig. 17. The curves shown in Fig. 17 indicate that for Da = 1×10^{-6} and 5×10^{-4}, L_L decreases slightly with increasing Re, while for Da = 7.4×10^{-3}, L_L initially decreases slightly and then increases with increasing Re. For a relative small Da ($= 5 \times 10^{-4}$), L_L becomes negative but rather close to zero for a certain range of Re, which means the recirculating wake slightly penetrates into the porous square cylinder. However, it is worth mentioning that the recirculating wake always initially develops downstream of the cylinder. Fig. 17 shows that, for fixed Da, with increasing Re, L_R increases linearly if Da = 1×10^{-6} and 5×10^{-4}, while L_R initially increases and then decreases if Da = 7.4×10^{-3}. Fig. 17 also indicates that for fixed Re, L_R always decreases with a decrease in Da. For fixed Re, with a decrease in Da, L_R increases when Re is less than $\sim$30 while may decreases if Re > $\sim$30.

The lengths of the recirculating wake L_w are plotted against Re with Da as a parameter in Fig. 18. Also, L_w for the solid cylinder obtained by the simulations of the present study and by the simulations and the formulation of Sharma and Eswaran (2004) at different Re are presented in Fig. 18. It is apparent, for the solid cylinder, the present results agree well with those of Sharma and Eswaran (2004) and only a small discrepancy exists when Re is large (Re > 40). Also, as in the case of L_R, with increasing Re, L_w linearly increases when Da is moderate ($= 5 \times 10^{-4}$) or small ($= 1 \times 10^{-6}$) while it initially increases and then decreases when Da is large ($= 7.4 \times 10^{-3}$). Generally, for fixed Re, the wake length increases with decreasing Da. However, when Re is large ($\sim$45), the wake length reaches its maximum ($\sim$3.27) when Da is around 5×10^{-4} as shown in Fig. 18.

Fig. 19 presents the position of the wake centre (C_x and C_y) against Re with Da as a parameter. For fixed Da, C_x always increases with increasing Re, which means that the wake centre moves downstream with increasing Re. The variation of C_y with Re is more complicated as shown in Fig. 19. For fixed Da, with increasing Re, C_y increases when Da is moderate ($= 5 \times 10^{-4}$) or small ($= 1 \times 10^{-6}$), while it initially increases and then decreases when Da is large ($= 7.4 \times 10^{-3}$). For fixed Re ($\leqslant 20$), C_x slightly increases with decreasing Da and approaches a constant when Da $\to$ 0. However, there is no general trend for the variation of C_x with Da when Re is larger than 25. As shown in Fig. 19, C_x reaches the maximum value at Da = 7.4×10^{-3} when Re = 30. For fixed Re, C_y increases with decreasing Da, which means that the wake becomes wider with decreasing Da. It is worth mentioning that for fixed Re ($\geqslant 35$), both C_x and C_y at different Da ($\leqslant 5 \times 10^{-4}$) appear to approach a constant value.

It is worth noting that the curves for Da = 7.4×10^{-3} in Figs. 17–19 demonstrate a different trend from those of Da = 5×10^{-4} and 1×10^{-6}. As shown before, with increasing Re, the recirculating wake first increases, then shrinks, and eventually disappears at Da = 7.4×10^{-3} while monotonically increases at Da = 5×10^{-4} and 1×10^{-6}. Thus, the variation of the geometry of recirculating wake with Re for Da = 7.4×10^{-3} behaves differently comparing with those for Da = 5×10^{-4} and 1×10^{-6}. The fundamental reason is vorticity accumulation as mentioned before. At Da = 5×10^{-4}, more vorticity is convected downstream of the cylinder due to more fluid penetrating through the cylinder. When the generation rate of vorticity is slower than the convection rate, the recirculating wake

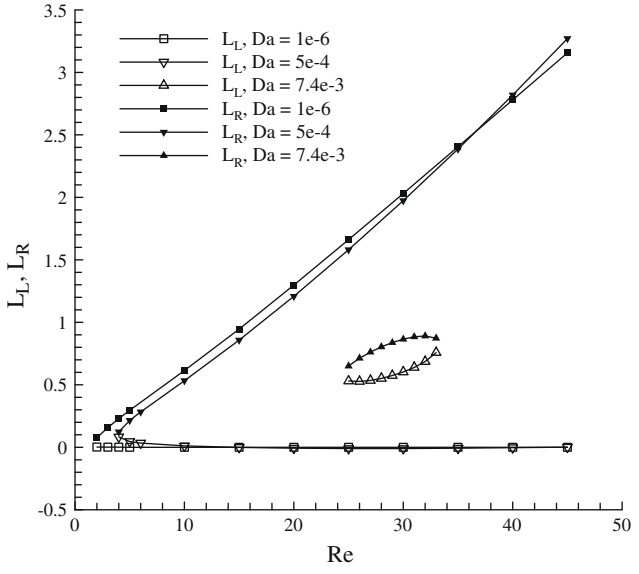

Fig. 17. Downstream distances to the leading and trailing edges of the recirculating wake (L_L and L_R) against Re with Da as a parameter.

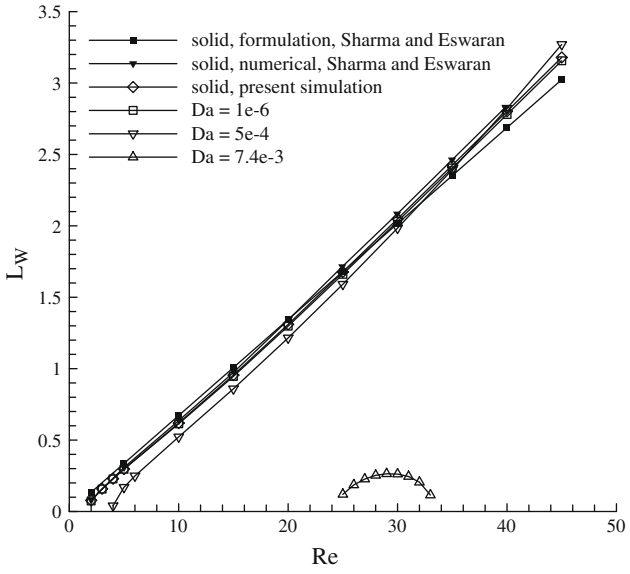

Fig. 18. Length of the recirculating wake L_w against Re with Da as a parameter.

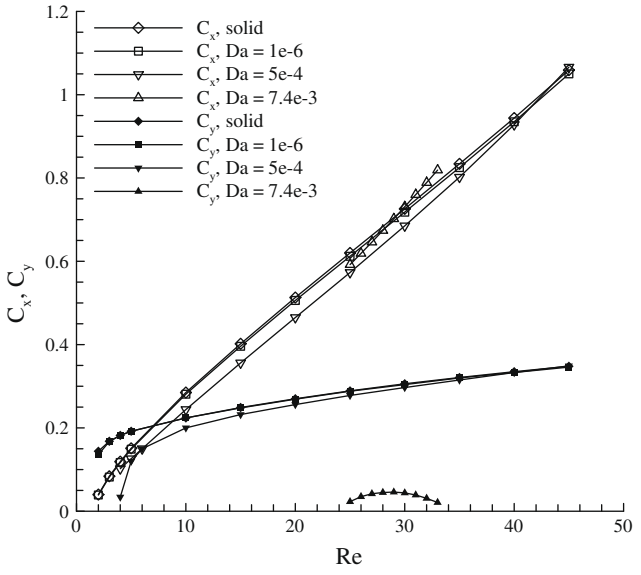

Fig. 19. Position of the wake centre (C_x and C_y) against Re with Da as a parameter.

may shrink or disappear. However, at the small Da (5×10^{-4} and 1×10^{-6}), the magnitude of vorticity is increased with increasing Re, thus increasing the size of the recirculating wake.

Figs. 17–19 show that, for fixed Re ($\leqslant 20$), the recirculating wake is displaced in the downstream direction while becoming both narrower and shorter with an increase in Da. Because an increase in Da means a big 'base bleed' rate, this wake behaviour is rather similar to that behind 2D bluff body with base bleed (Leal and Acrivos, 1969). Other wake behaviours associated with variations of Da and Re are also similar to the findings of Leal and Acrivos (1969), which include that for fixed Re ($\leqslant 20$), C_y and L_R decrease with increasing Da.

Figs. 18 and 19 also suggest that for fixed Da, especially when Da is small, the characteristic dimensions of the recirculating wake behind the porous cylinder are the same order of that behind the solid cylinder at the same Re. This in turn suggests that although the detached recirculating wake is more complicated than the attached wake behind a solid cylinder, the dependence of its geometric parameters on Reynolds number seems to remain qualitatively unchanged, especially for a small Da. Again, this conclusion is consistent with that of Leal and Acrivos (1969).

However, there are also noticeable differences between the present simulations and the observations of Leal and Acrivos (1969). With increasing Da, the recirculating centre moves upstream for a small Re ($\leqslant 20$) in the present study but downstream observed by Leal and Acrivos (1969). Obviously, the present flow is more complicated than that of Leal and Acrivos (1969), and thus cannot be only completely explained from the point of view of base bleed. Fig. 16 have shown that, for fixed Da, with increasing Re, the 'base bleed' rate increases when $Da > 5 \times 10^{-3}$ while decreases when $Da < 1 \times 10^{-3}$. This result suggests that the detached wake can be only understood from the interaction between the external flow around and the internal flow within the porous square cylinder.

For the external flow around a solid square cylinder, the flow is mainly determined by the Reynolds number. The magnitude of vorticity on the surface of cylinder and the wake length increase with increasing Re. With the presence of base bleed, the convection of the vorticity becomes increasingly efficient. The recirculating wake is displaced in the downstream direction while becoming both narrower and shorter with increasing base bleed rate as shown by Leal and Acrivos (1969). The present wake behaviour results from vorticity accumulation due to the competition/cooperation of Re-effect and Da-effect.

Table 2
Effect of porosity on the overall wake length; $Da = 5 \times 10^{-6}$, Re = 20, $\beta_1 = \beta_2 = 0$.

Porosity	0.4	0.5	0.6	0.7	0.8	0.9
L_R	1.300	1.298	1.296	1.294	1.293	1.291

Table 3
Effect of jump parameters on the overall wake length; $Da = 5 \times 10^{-6}$, Re = 20, $\varepsilon = 0$.

β_1	0	0	0	1.0	1.0	1.0
β_2	−1.0	0	1.0	−1.0	0	1.0
L_R	1.293	1.294	1.294	1.303	1.303	1.304

For the case of a porous square cylinder, the 'base bleed' rate through the leeward surface is affected by both Da and Re. As indicated by Eq. (3), the 'base bleed' rate increases with increasing Re and/or Da, which explains that the 'base bleed' rate increases with increasing Re at fixed Da ($> 5 \times 10^{-3}$). However, when Da is less than 1×10^{-3}, Fig. 16 shows that the 'base bleed' rate decreases with increasing Re at fixed Da. For a small value of Da, the 'base bleed' rate is small, which has less effect on the external flow. Thus, the wake structure is mainly determined by Re. With increasing Re, the rate of vorticity production on the surface increases more efficiently than that of vorticity convection downstream. As a result, the recirculating wake moves upstream and expands in size with increasing Re as shown in Figs. 17–19. When Da is small, the recirculating wake is rather close to the rear of square cylinder, which blocks the base bleed from the leeward surface. Thus, the 'base bleed' rate decreases with increasing Re at a small value of Da ($< 1 \times 10^{-3}$) due to this 'block' effect as shown in Fig. 16. When Da is large ($> 5 \times 10^{-3}$), the recirculating wake is relatively far from the cylinder, and the 'block' effect is negligible.

For fixed Re, the 'base bleed' rate increases with Da, which means that the amount of fluid passing around the cylinder decreases. This implies a decrease in the effective Reynolds number Re_{eff} as discussed above. Thus, with increasing Da, the recirculating wake becomes narrower and shorter due to both 'base bleed' effect and Re_{eff} effect.

For a relative large Re ($Re > 35$), Figs. 17–19 suggest that the wake geometry is not sensitive to the variation of Da ($\leqslant 5 \times 10^{-4}$). As explained above, for a large Re, the detached wake is rather close to the rear of cylinder when $Da \leqslant 5 \times 10^{-4}$. The 'base bleed' rate is almost constant due to the 'block' effect of the wake. Thus, the wake structure remains unchanged when Da is varied.

It is known that besides Re and Da, other parameters, such as jump coefficients, porosity may also affect the flow. Tables 2 and 3 summarize the variation of the overall wake length L_R with different porosities and jump parameters respectively. The two tables show that the effects of porosity and jump parameters on L_R are negligibly small.

4. Conclusion

The present study examines the detailed wake structure behind a permeable square cylinder over a wide range of parameters. The present simulations reveal that the recirculating wake existing behind the porous square cylinder is detached from the cylinder, but is not attached to the cylinder as which occurs behind a solid cylinder. The recirculating wake is found to develop downstream of the porous cylinder, but not from its surface as that of the solid cylinder. Also, there is only one "separation" point along the horizontal axis, but not a pair of separation points on the surface of the

solid cylinder. When Da → 0, the wake behaviour of the porous cylinder resembles that of the solid one, which suggests the underlying physics of the detached or penetrating wake behind the porous cylinder may be the same as that of the solid one. All these features support the conclusion of Leal (1989) that the existence of recirculating wake behind any body at large, but finite Reynolds number should be regarded as being a consequence of the accumulation of vorticity generated upstream on the body surface.

The present wake behaviour can be explained from interaction between the external flow around and the internal flow within the porous square cylinder. Obviously, the Reynolds number has an important effect on the wake structure. Also, the 'base bleed' rate along the leeward surface of the porous cylinder is affected by both Re and Da, thus influencing the recirculating wake structure. The wake structure in turn affects the 'base bleed' rate, due to the 'block' effect. Specially, the wake structure may also be influenced by the change of the effective Reynolds number due to the 'base bleed' effect. The final wake structure is determined by the balance of all the effects.

The present results, together with the previous results for the porous circular cylinder (Yu et al., submitted for publication), confirm that the detached wake is an inherent, but not a hypothetical, phenomenon associated with the flow past and around the porous cylinder, which appears to control by the weak motion of the fluid passing through the porous body. This promotes follow-up study to re-evaluate the case of porous sphere from the point of view of the effect of the internal porous flow on the external flow. Note that only steady flow is considered in the present study. It would be also interesting to further investigate the time-dependent flow behaviour around and through the porous square cylinder.

References

Arcas, D.R., Redekopp, L.G., 2004. Aspects of wake vortex control through base blowing/suction. Phys. Fluids 16, 452–456.

Bearman, P.W., 1967. The effect of base bleed on the flow behind a two-dimensional model with a blunt trailing edge. Aeronaut. Quart. 18, 207–224.

Bhattacharyya, S., Dhinakaran, S., Khalili, A., 2006. Fluid motion around and through a porous cylinder. Chem. Eng. Sci. 61, 4451–4461.

Braeckmans, K., De Smedt, S.C., Leblans, M., Pauwels, R., Demeester, J., 2002. Encoding microcarriers: present and future technologies. Nat. Rev. Drug Discov. 1, 447–456.

Chen, X.B., Yu, P., Winoto, S.H., Low, H.T., 2008. Numerical analysis for the flow past a porous square cylinder based on the stress-jump interfacial-conditions. Int. J. Numer. Meth. Heat Fluid Flow 18, 635–655.

Dandy, D., Leal, L.G., 1986. Boundary-layer separation from a smooth slip surface. Phys. Fluids 29, 1360–1366.

Dandy, D., Leal, L.G., 1989. Buoyancy driven motion of a deformable drop through a quiescent liquid at intermediate Reynolds numbers. J. Fluid Mech. 208, 161–192.

Ferziger, J.H., Perić, M., 1999. Computational Methods for Fluid Dynamics, second ed. Springer, Berlin.

Joseph, D.D., Tao, L.N., 1964. The effect of permeability on the slow motion of a porous sphere in a viscous liquid. Z. Angew. Math. Mech. 44, 361–364.

Jue, T.C., 2004. Numerical analysis of vortex shedding behind a porous cylinder. Int. J. Numer. Meth. Heat Fluid Flow 14, 649–663.

Large, J.L., 1992. Effect of the convective inertia term on bénard convection in a porous medium. Numer. Heat Transfer A 22, 469–485.

Leal, L.G., 1989. Vorticity transport and wake structure for bluff-bodies at finite Reynolds-number. Phys. Fluids A-Fluid 1, 124–131.

Leal, L.G., Acrivos, A., 1969. The effect of base bleed on the steady separated flow past bluff objects. J. Fluid Mech. 38, 735–752.

Lilek, Ž., Muzaferija, S., Perić, M., Seidl, V., 1997. An implicit finite-volume method using nonmatching blocks of structured grid. Numer. Heat Transfer B-Fund. 32, 385–401.

Masliyah, J.H., Polikar, M., 1980. Terminal velocities of porous spheres. Can. J. Chem. Eng. 58, 299–302.

Neale, G., Epstein, N., Nadar, W., 1973. Creeping flow relative to permeable spheres. Chem. Eng. Sci. 28, 1865–1874.

Noymer, P.D., Glicksman, L.R., Devendran, A., 1998. Drag on a permeable cylinder in steady flow at moderate Reynolds numbers. Chem. Eng. Sci. 53, 2859–2869.

Ochoa-Tapia, J.A., Whitaker, S., 1995a. Momentum transfer at the boundary between a porous medium and a homogeneous fluid I: theoretical development. Int. J. Heat Mass Transfer 38, 2635–2646.

Ochoa-Tapia, J.A., Whitaker, S., 1995b. Momentum transfer at the boundary between a porous medium and a homogeneous fluid II: comparison with experiment. Int. J. Heat Mass Transfer 38, 2647–2655.

Ochoa-Tapia, J.A., Whitaker, S., 1998. Momentum jump condition at the boundary between a porous medium and a homogeneous fluid: inertial effect. J. Porous Media 1, 201–217.

Rivkind, V.Y., Ryskin, G.M., 1976. Flow structure in motion of a spherical drop in a fluid medium at intermediate Reynolds numbers. Fluid Dyn. 11, 5–12.

Sharma, A., Eswaran, V., 2004. Heat and fluid flow across a square cylinder in the two-dimensional laminar flow regime. Numer. Heat Transfer A-Appl. 45, 247–269.

Sohankar, A., Norberg, C., Davidson, L., 1998. Low-reynolds-number flow around a square cylinder at incidence. study of blockage, onset of vortex shedding and outlet boundary condition. Int. J. Numer. Meth. Fluids 26, 39–56.

Underwood, R.L., 1969. Calculation of incompressible flow past a circular cylinder at moderate Reynolds numbers. J. Fluid Mech. 37, 95–114.

Yu, P., Lee, T.S., Zeng, Y., Low, H.T., 2007. A numerical method for flows in porous and open domains coupled at the interface by stress jump. Int. J. Numer. Meth. Fluid 53, 1755–1775.

Yu, P., Lee, T.S., Zeng, Y., Low, H.T., 2009. Fluid dynamics and oxygen transport in a micro-bioreactor with a tissue engineering scaffold. Int. J. Heat Mass Transfer 52, 316–327.

Yu, P., Zeng, Y., Lee, T.S., Chen, X.B., Low, H.T., submitted for publication. Steady flow around and through a permeable circular cylinder. Comput. Fluids.

Zaki, T.G., Sen, M., Gad-el-Hak, M., 1994. Numerical and experimental investigation of flow past a freely rotatable square cylinder. J. Fluid Struct. 8, 555–582.